22nd International Conference on Sustainable Energy Technologies
Kuala Lumpur, Malaysia, 13 to 15 August 2026 · ISBN 978-1-995850-00-9 · ISSN 2978-4387

CONFERENCE PAPER · ENERGY STORAGE & CONVERSION

A novel salt hydrate thermochemical Rankine-Carnot battery: system design, heat exchanger network integration, and thermodynamic assessment

Xianmin Zeng[1]*, Xianglong Luo[1], Yingzong Liang[1], Jianyong Chen[1], Zhi Yang[1], Rongjun Wu[1]

[1] School of Materials and Energy, Guangdong University of Technology, Guangzhou, China

RECEIVED 30 April 2026 · REVISED 26 May 2026 · ACCEPTED 8 June 2026
PRESENTED 13 to 15 August 2026 · PUBLISHED 23 November 2026

ABSTRACT

The increasing penetration of renewable energy has created a growing demand for large-scale and long-duration energy storage technologies with high efficiency and flexible deployment. Thermochemical Carnot batteries are promising candidates because they can store energy in a chemical form with low heat loss and high energy density. However, most existing thermochemical Carnot battery studies focus on medium and high temperature materials, while medium and low temperature salt-hydrate systems remain insufficiently explored. In this study, a two-stage compression Carnot battery system with heat exchanger networks (TSC-CB-HEN) was proposed and thermodynamically assessed, with $CaCl_2{\cdot}2H_2O$/$CaCl_2{\cdot}H_2O$ employed as the thermochemical energy storage material. The system integrates a heat pump cycle, thermochemical energy storage, organic Rankine cycle (ORC), two-stage compression, and charging/discharging heat exchanger networks. A steady-state thermodynamic model was established to analyse mass, energy, and exergy balances, while the dehydration pressure, hydration pressure, and ORC evaporation temperature were optimized to improve the round-trip efficiency. Pinch analysis was further applied to guide the design of the charging and discharging heat exchanger networks. The results show that the optimal operating condition corresponds to a dehydration pressure of 4 kPa, a hydration pressure of 80 kPa, and an ORC evaporation temperature of 150 °C. Compared with the Salt-Hydrate Carnot Battery System (SH-CB), the TSC-CB-HEN increased the heat pump COP from 3.032 to 3.581 and the round-trip efficiency from 44.18% to 53.71%. The system exergy efficiency reached approximately 63.6%, while the total exergy destruction was 604.24 kW. The largest exergy destruction occurred in HEX2, accounting for 34.9% of the total, mainly due to temperature mismatch during internal heat recovery and reactant preheating. These results show that pressure regulation, two-stage compression, and heat exchanger network integration can effectively enhance the energy conversion performance of thermochemical Carnot batteries.

KEYWORDS Rankine-Carnot battery, Salt hydrate, Thermochemical energy storage, Heat exchanger network, Exergy analysis

1. Introduction

In recent years, global energy demand has continued to increase, while fossil fuels such as coal, oil, and natural gas still dominate the energy supply. As a result, energy-related CO_2 emissions have remained high. According to the International Energy Agency (IEA), global energy-related CO_2 emissions increased by 0.8% in 2024, reaching a record high of 37.8 Gt (IEA 2025). Meanwhile, the growth of electrification, industrial production, data centers, and cooling demand has further increased global electricity demand, placing greater pressure on the low-carbon transition of energy systems. To address the dual pressures of increasing energy demand and carbon emission constraints, the global energy system is accelerating its transition toward low-carbon development,

* Corresponding author. Email address: 553196043@qq.com (Xianmin Zeng)

© 2026 The Author(s).
Published by Caravel Press.

doi.org/10.65582/set.2026.008

with the share of renewable energy sources such as wind and solar power continuing to increase in the energy mix (Huang *et al.* 2025).

However, the large-scale utilization of renewable energy is limited by intermittency and spatiotemporal mismatch between supply and demand (Tariq and Amin 2025; Li *et al.* 2024b). Therefore, energy storage technologies have attracted increasing attention. Among various storage methods, thermal energy storage has advantages such as abundant storage media, flexible capacity, long service life, and low cost, making it suitable for large-scale and long-duration energy storage. The Carnot battery is a thermal-energy-storage-based technology that converts electricity into heat during charging and converts stored heat back into electricity during discharging through a heat engine cycle (Dumont *et al.* 2020). According to the storage mechanism, Carnot batteries can be classified into sensible heat, latent heat, and thermochemical energy storage systems (Vecchi *et al.* 2022). Among them, thermochemical Carnot batteries have high energy storage density, low heat loss, and long storage duration, showing great potential for long-term energy storage.

Existing studies on thermochemical Carnot batteries mainly focus on materials, reactors, and system integration. At the material level, research has investigated reaction enthalpy, equilibrium temperature, energy storage density, cycling stability, and reversibility. $Ca(OH)_2/CaO$ has been widely studied because of its high energy storage density, good reversibility, and abundant availability (Kur *et al.* 2023; Pardo *et al.* 2014). Compared with medium- and high-temperature materials, salt hydrates generally have lower dehydration temperatures, and their equilibrium temperatures can be adjusted by water vapor pressure, making them promising for medium- and low-temperature thermochemical energy storage (Hayatina *et al.* 2023). In particular, the $CaCl_2{\cdot}2H_2O/CaCl_2{\cdot}H_2O$ reaction pair has advantages such as low cost, abundant availability, high hydration heat, and strong pressure-regulation characteristics. Previous studies have demonstrated the dehydration/hydration behavior, reaction pathway, and thermal transformation potential of $CaCl_2$ hydrates (Pathak *et al.* 2016; Kato *et al.* 2024; Molenda *et al.* 2013; Richter *et al.* 2016), indicating their suitability for medium- and low-temperature salt-hydrate thermochemical Carnot batteries.

At the reactor level, thermochemical storage materials are usually solid particles or porous media, and their performance is strongly affected by heat and mass transfer, gas–solid contact, and bed temperature distribution. Therefore, reactor optimization and heat-transfer enhancement are important for improving charging and discharging rates. Studies on fluidized-bed reactors and fin-enhanced reactors have shown that appropriate reactor structures can improve heat transfer, increase reaction conversion, and enhance system dynamic performance (Pardo *et al.* 2014; Zhao *et al.* 2024).

At the system level, existing studies mainly couple thermochemical storage units with heat pump cycles, power cycles, and heat exchanger networks. $Ca(OH)_2/CaO$-based thermochemical Carnot batteries coupled with supercritical CO_2 Brayton heat-pump and power cycles have achieved round-trip efficiencies as high as 71.52% after optimization (Zhang *et al.* 2025). The coupling of $Ca(OH)_2/CaO/CaCO_3$ thermochemical storage with supercritical CO_2 cycles and CO_2 capture further broadens system functionality toward energy storage, heat supply, and carbon capture (Li *et al.* 2024b). For salt-hydrate-based Carnot batteries, recuperation has been shown to increase the power-to-power efficiency from 48.48% to 64.1% and reduce the levelized cost of storage from 0.2502 to \$0.1922/kWh (Risthaus *et al.* 2022).

Although significant progress has been made in thermochemical Carnot batteries, most system-level studies focus on medium and high temperature materials, such as $Ca(OH)_2/CaO$ and $CaCO_3/CaO$, coupled with Brayton or supercritical CO_2 cycles. Research on medium- and low-temperature salt-hydrate thermochemical Carnot batteries remains limited, especially considering their complex heat integration involving condensation, evaporation, reactant preheating, and product cooling. Therefore, this paper proposes a $CaCl_2{\cdot}2H_2O/CaCl_2{\cdot}H_2O$ salt-hydrate thermochemical Carnot battery coupled with two-stage compression heat pump, organic Rankine cycle, and heat exchanger networks. By regulating water vapor pressure and enhancing internal heat recovery, the proposed

system enables low-temperature energy storage, higher-temperature heat release, and improved overall performance.

2. System description

2.1. Salt-hydrate Carnot battery system (SH-CB)

As shown in Fig. 1(a), the system is a salt-hydrate Carnot battery system, mainly consisting of a heat pump cycle, a thermochemical energy storage module, and an Organic Rankine Cycle. The thermochemical energy storage module includes a dehydration reactor, a hydration reactor, an auxiliary compressor, a water pump, and storage tanks. Both the dehydration and hydration reactors adopt a fluidized-bed configuration. Compared with fixed-bed reactors, fluidized-bed reactors exhibit superior heat and mass transfer characteristics (Liu *et al.* 2025). Fig. 1(b) shows the temperature-entropy (T-s) diagrams, which describe the charging and discharging processes of this system.

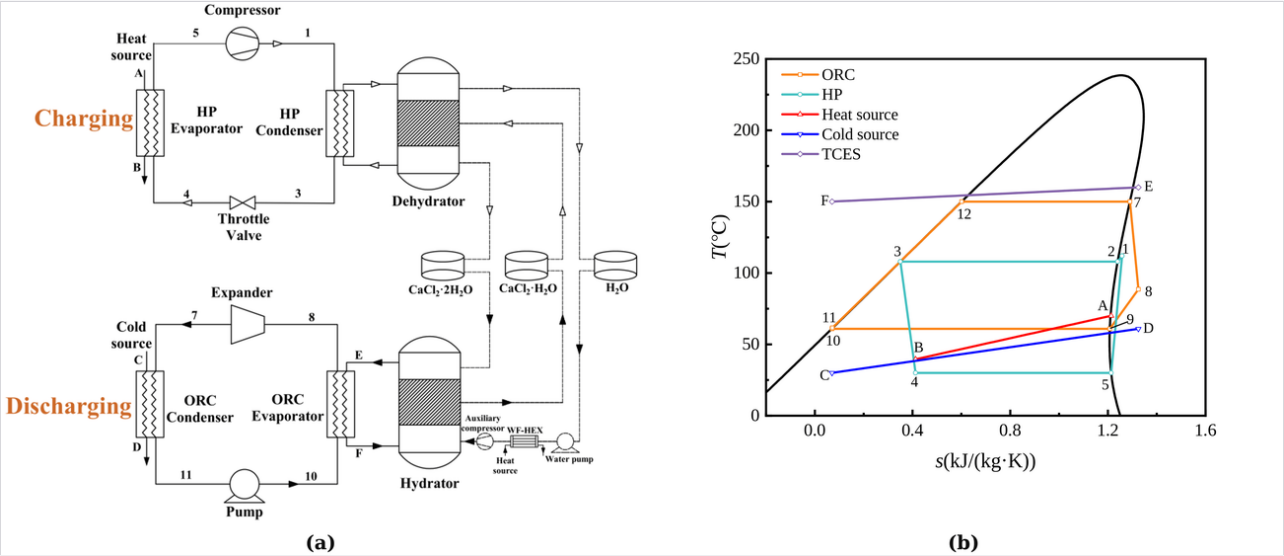

Figure 1. (a) Schematic of the salt-hydrate Carnot battery system, (b) T-s diagram of the SH-CB.

During the charging process, pressurized water is used as the heat transfer fluid to transfer heat from the heat pump to the dehydration reactor, thereby driving the dehydration reaction of the salt hydrate. As a result, electrical energy is converted into chemical energy and thermal energy for storage. The generated water vapor is condensed, and the condensed water and dehydrated salt are stored separately for the subsequent discharging process. During the discharging process, the stored liquid water is pressurized, evaporated, and further compressed before entering the hydration reactor. The water vapor then reacts with the dehydrated salt to regenerate the hydrated salt and release high-grade heat, which is supplied to the ORC working fluid for power generation. After expansion in the turbine, the ORC working fluid rejects heat to the cold source in the condenser and is pumped back to the evaporator, completing the ORC cycle.

By regulating the water vapor pressure, the dehydration/hydration equilibrium temperature can be adjusted, enabling low-temperature energy storage and higher-temperature heat release. However, the basic system suffers from insufficient recovery of sensible and latent heat and high power consumption caused by single-stage compression. Therefore, two-stage compression and heat exchanger networks are introduced to improve internal heat recovery, enhance energy cascade utilization, and increase the round-trip efficiency.

2.2. Two-stage compression Carnot battery system with heat exchanger networks (TSC-CB-HEN)

To address these limitations, an improved thermochemical Carnot battery system integrating two-stage compression and heat exchanger networks is proposed, as shown in Fig. 2(a). Compared with the basic configuration, the improved system introduces two-stage compression and heat exchanger networks on both the charging and discharging. This system reduces the pressure ratio and power consumption, while the heat exchanger networks enhance internal heat recovery and heat matching within the TCES module. The corresponding T–s diagrams are shown in Fig. 2(b).

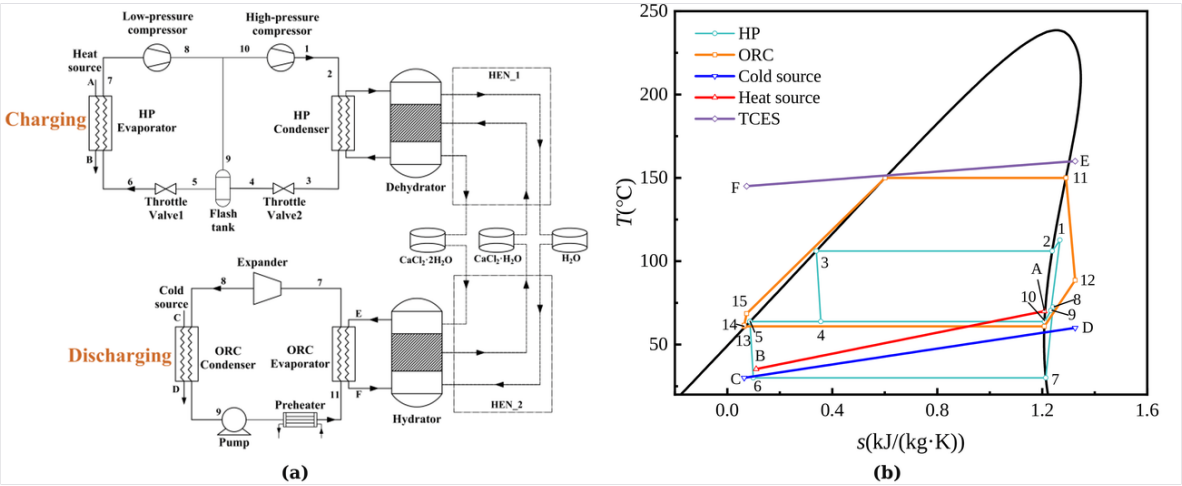

Figure 2. (a) Schematic of the TSC-CB-HEN, (b) T-s diagram of TSC-CB-HEN.

In salt-hydrate Carnot battery systems, the charging and discharging processes involve not only reaction heat absorption and release but also water vapor condensation, liquid water evaporation, and product cooling, which generate considerable sensible and latent heat. Heat exchanger networks are therefore introduced to recover and reuse this internal heat, reducing energy and exergy losses while improving heat cascade utilization.

During the charging process, the heat pump adopts a two-stage compression configuration to reduce compression power consumption. Meanwhile, the charging heat exchanger network recovers heat from dehydration products and water vapor condensation, which is then used to preheat the solid reactants entering the dehydration reactor, thereby reducing the heat supply required from the heat pump. During the discharging process, the heat exchanger network recovers heat from hydration products and internal circulating streams. The recovered heat is used to preheat the reactants entering the hydration reactor and the ORC working fluid before the main evaporator, thereby improving heat matching, reducing the ORC evaporator load, and enhancing the thermal efficiency of the ORC.

3. Methods

3.1. Conditions and assumptions

A steady-state thermodynamic model is established to simulate the mass and energy balances of each component. Owing to its favorable thermodynamic performance, environmental compatibility, and relatively high critical temperature, cyclopentane is selected as the working fluid for both the heat pump cycle and the ORC, as it can satisfy the temperature requirements of the charging and discharging processes. The main parameters of the heat pump cycle are listed in Table 1.

Table 1. Main parameters of the heat pump cycle.

Parameter	Component/streams	Value
Power input during charging	-	0.4 MW
Isentropic efficiency	Compressor	0.86
	Turbine	0.86
Pinch temperature difference	-	5 °C
Evaporation temperature	Cyclopentane	30 °C
Temperature limit	Flue gas	80 °C
Heat supply temperature	HTF	110 °C
Cold source temperature	Air	30 °C

In the TCES module, $CaCl_2 \cdot 2H_2O$ is employed as the thermochemical material. The dehydration/hydration reaction follows the Clausius-Clapeyron relationship, and the monovariant characteristic equilibrium curve of the gas–solid reaction is described by:

$$\ln\left(\frac{p_{eq}}{p_{ref}}\right) = -\frac{\Delta H_r}{RT_{eq}} + \frac{\Delta S_r}{R} \tag{1}$$

Where:

- p_{eq} = equilibrium water vapor partial pressure (kPa)
- p_{ref} = reference pressure (kPa)
- T_{eq} = equilibrium temperature (K)
- ΔH_r = reaction enthalpy change (kJ/mol)
- ΔS_r = reaction entropy change (J/(mol·K))
- R = universal gas constant (J/(mol·K))

The charging and discharging reactions are described by Eq. (2), and the corresponding parameters are listed in Table 2. The thermophysical properties of the working fluids are obtained from the NIST REFPROP database, while those of $CaCl_2 \cdot 2H_2O$ and $CaCl_2 \cdot H_2O$ are taken from the Aspen Plus database.

Table 2. Parameters of the auxiliary machines and heat transfer.

Parameter	Component/streams	Value	Ref.
Heat transfer coefficient	Gas	600 W/(m²·K)	(Albrecht and Ho 2019)
	Solid particle	200 W/(m²·K)	
	Water	2500 W/(m²·K)	
Hydraulic efficiency	Water pump	0.75	
Mechanical efficiency	Water pump	0.97	
Pressure limit	Auxiliary compressor	3	(Li *et al.* 2024b)

$$CaCl_2 \cdot 2H_2O_{(s)} + \Delta H_r \underset{\text{discharging}}{\overset{\text{charging}}{\longleftrightarrow}} CaCl_2 \cdot H_2O_{(s)} + H_2O_{(g)} \tag{2}$$

The auxiliary electrical energy required for material transportation is neglected with reference to the literature, and heat losses are ignored. The main assumptions are as follows:

(1) During the charging and discharging processes, the thermophysical properties and reaction enthalpy of the reactive salt remain unchanged (Risthaus *et al.* 2022).

(2) The isentropic efficiencies of the expander, compressors, and pumps are assumed to be constant (Liu *et al.* 2025).

(3) Heat losses and pressure drops during heat transfer processes are neglected (Wang *et al.* 2024).

(4) Agglomeration and deliquescence of the reactive salt are neglected (Li *et al.* 2024b).

3.2. Simulation models

As one of the most important indicators for assessing systems, round-trip efficiency (η_{rt}) is formulated as follows:

$$\eta_{rt}=\frac{P_{output}}{P_{input}+\sum P_{aux}} \tag{3}$$

Where:

- P_{output} = net output power of the system during the discharging process (kW)
- P_{input} = power input from the grid during the charging process (kW)
- P_{aux} = total power consumption of the auxiliary equipment (kW)

The coefficient of performance (COP) of the HP cycle is calculated by:

$$COP = \frac{Q_{HP}}{P_{input}} \tag{4}$$

Where:

- Q_{HP} = heat transferred outward by the heat pump condenser during the charging process (kW)
- P_{HP} = input power of the heat pump cycle (kW)

The η_{ORC}, which means the thermal efficiency of the ORC, is expressed as follows:

$$\eta_{ORC} = \frac{P_{ORC}}{Q_{ORC}} \tag{5}$$

Where:

- P_{ORC} = effective power output during the ORC discharging power generation process (kW)
- Q_{ORC} = heat absorbed by the ORC evaporator during the discharging process (kW)

Exergy efficiency, according to the second law of thermodynamics, means a system's maximum potential to perform useful work and is therefore a key performance metric. It can be described by:

$$\eta_{ex} = \frac{Ex_{output} + Q_{re1}\left(1 - \frac{T_0}{T_{ch1}}\right)}{Ex_{input} + \sum Ex_{aux}} \tag{6}$$

Where:

- Ex_{output} = output exergy of the system (kW)
- Ex_{input} = input exergy of the system (kW)
- T_0 = ambient temperature (K)
- T_{ch1} = charging temperature of the reactor (K)

The exergy of the working fluid is obtained by:

$$Ex_{fc} = m_{fc} \cdot \left[h_{fc} - h_0 - T_0\left(s_{fc} - s_0\right)\right] \tag{7}$$

Where:

- Ex_{fc} = physical exergy of the fluid (kW)
- m_{fc} = mass flow rate of the fluid (kg/s)
- h_{fc} = specific enthalpy of the fluid at the current state (kJ/kg)
- h_0 = specific enthalpy at the environmental reference state (kJ/kg)
- s_{fc} = specific entropy of the fluid at the current state (kJ/(kg·K))
- s_0 = specific entropy at the environmental reference state (kJ/(kg·K))

The exergy destruction (Ex_d) of the component can be determined as below:

$$Ex_d = Ex_{in} - Ex_{out} \tag{8}$$

Where:

- Ex_{in} = total exergy input to the component (kW)
- Ex_{out} = total exergy output of the component (kW)

Table 3. Energy balance and exergy destruction equations for equipment in the system.

Component	Energy Balance	Exergy destruction (Ex_d)
HP Evaporator	$Q_{flue} = m_{HP} \cdot (h_7 - h_6)$	$Ex_{flue,\,in} - Ex_{flue,\,out} + Ex_6 - Ex_7$
Compressor 1	$W_{com1} = m_{HP} \cdot (h_8 - h_7)$	$W_{com1} + Ex_7 - Ex_8$
Compressor 2	$W_{com2} = m_{HP} \cdot (h_1 - h_9)$	$W_{com2} + Ex_9 - Ex_1$
REC1	$m_{HP} \cdot (h_1 - h_9) = m_{HTF} \cdot (h_C - h_D)$	$Ex_9 - Ex_1 + Ex_D - Ex_C$
Throttle 1	$h_3 = h_4$	$Ex_4 - Ex_3$
Throttle 2	$h_5 = h_6$	$Ex_6 - Ex_5$
Flash tank	$h_4 = \varphi h_{10} + (1 - \varphi)h_5$	$Ex_4 - (1 - \varphi)Ex_5 + Ex_4 - \varphi Ex_{10}$
REC2	$m_{HTF} \cdot (h_E - h_F) = m_{ORC} \cdot (h_{11} - h_{15})$	$Ex_F - Ex_E + Ex_{15} - Ex_{11}$
Expander	$W_{exp} = m_{ORC} \cdot (h_{11} - h_{12})$	$Ex_{12} - Ex_{11} - W_{exp}$
ORC condenser	$m_{ORC} \cdot (h_{12} - h_{13}) = m_{air} \cdot (h_{in} - h_{out})$	$Ex_{air,\,in} - Ex_{air,\,out} + Ex_{13} - Ex_{12}$

Table 3 summarizes concrete expressions regarding energy and exergy. In this study, the system round-trip efficiency is selected as the optimization objective, and a sequential quadratic programming algorithm is employed to optimize the SH-CB and TSC-CB-HEN. During the optimization process, the dehydration reaction pressure, hydration reaction pressure, and ORC evaporation temperature are selected as independent variables. The ranges of these optimization variables are listed in Table 4.

Table 4. Ranges of optimization variables.

Optimization variable	Lower bound	Upper bound	Unit
Dehydration reaction pressure	3	10	kPa
Hydration reaction pressure	40	100	kPa
ORC evaporation temperature	100	150	°C

3.3. Model validation

To verify the heat pump cycle, the calculated results were compared with literature data, as shown in Table 5. Under the same heat source temperatures, evaporator superheat, heating production temperature, pinch point temperature difference, working fluid, and intermediate pressure calculation method, the COP calculated in this study is 3.468, close to the literature value of 3.285, with a relative error of 5.57%. This deviation is acceptable and may result from differences in property databases and state point calculations. Therefore, the established heat pump model is considered reliable for subsequent system performance analysis.

Table 5. Comparison of the results of this heat pump cycle with values from literature (Wang *et al.* 2025).

Parameter	Literature	Present system	Relative error
Heat source inlet temperature (°C)	90	90	-
Heat source outlet temperature (°C)	80	80	-
Evaporator superheat (°C)	15	15	-
Heating production temperature (°C)	150	150	-
Pinch point temperature difference (°C)	5	5	-
Working fluid	R601	R601	-
Intermediate parameters	$p_{im}=\sqrt{p_e p_c}$	$p_{im}=\sqrt{p_e p_c}$	-
COP	3.285	3.468	5.57%

To verify the ORC model, the calculated results were compared with literature data for a P-TCES system, as shown in Table 6. Under the same expander efficiency, pump efficiency, cold source temperature, pinch point temperature difference, heat supply temperature, and working fluid, the ORC efficiency calculated in this study is 13.59%, close to the literature value of 13.19%, with a relative error of 3.03%. This agreement indicates that the established ORC model is reliable for subsequent thermodynamic analysis.

Table 6. Comparison of the results of this ORC with values from literature (Li *et al.* 2024b).

Parameter	Literature	Present system	Relative error
Expander isentropic efficiency	0.9	0.9	-
Pump efficiency	0.85	0.85	-
Cold source temperature (°C)	20	20	-
Pinch point temperature difference (°C)	3	3	-
Hydration reaction heat supply temperature (°C)	100	100	-
Working fluid	R245fa	R245fa	-
ORC efficiency (%)	13.19	13.59	3.03%

4. Results and discussion

4.1. System optimization results

The system optimization results are presented in Table 7. The optimal operating condition is obtained at a dehydration pressure of 4 kPa, a hydration pressure of 80 kPa, and an ORC evaporation temperature of 150 °C. Under the optimized condition, the system COP increases from 3.032 to 3.581, with an improvement of 18.11%. The ORC efficiency also increases slightly from 14.5% to 15.0%, mainly due to the higher ORC evaporation temperature and improved heat matching on the discharging side. As a result, the round-trip efficiency increases from 44.18% to 53.71%, corresponding to an improvement of 21.57%. These results show that the combination of pressure regulation, two-stage compression, and ORC evaporation temperature optimization can effectively enhance the energy conversion performance of the salt-hydrate thermochemical Carnot battery system.

Table 7. Optimization results of the proposed thermochemical Carnot battery system.

Optimization variable	SH-CB	TSC-CB-HEN	Unit
Dehydration reaction pressure	4	4	kPa
Hydration reaction pressure	80	80	kPa
ORC evaporation temperature	150	150	°C
COP	3.032	3.581	-
ORC efficiency (%)	14.5%	15.0%	-
η_{rt}	44.18%	53.71%	-

4.2. Design of heat exchanger networks in the charging subsystem

As shown in Fig. 3, pinch analysis was conducted for HEN1 to identify the heat recovery potential and guide the design of the charging-side heat exchanger network. The hot streams mainly include the dehydration products, $CaCl_2{\cdot}H_2O$ and H_2O, while the cold stream is the reactant $CaCl_2{\cdot}2H_2O$ that needs to be preheated before entering the dehydrator. The small temperature difference in the high-temperature region indicates that part of the sensible and latent heat from the dehydration products can be recovered for reactant preheating. However, the large heat load near 25–30 °C shows that some released heat is at a low temperature level and is difficult to directly match with the high-temperature heat demand. Based on the grand composite curve in Fig. 3(b), the charging-side heat integration is mainly limited by low-temperature heat release. Therefore, the HEN1 configuration shown in Fig. 4 was designed. In this network, SS-HEXs recover sensible heat between the solid product $CaCl_2{\cdot}H_2O$ and the solid reactant $CaCl_2{\cdot}2H_2O$, while SW-HEXs recover heat between the solid streams and the water stream through an intermediate heat-transfer fluid. The remaining low-temperature heat is removed by air cooling. Overall, HEN1 enhances internal heat recovery and reduces the external heat demand of the dehydrator.

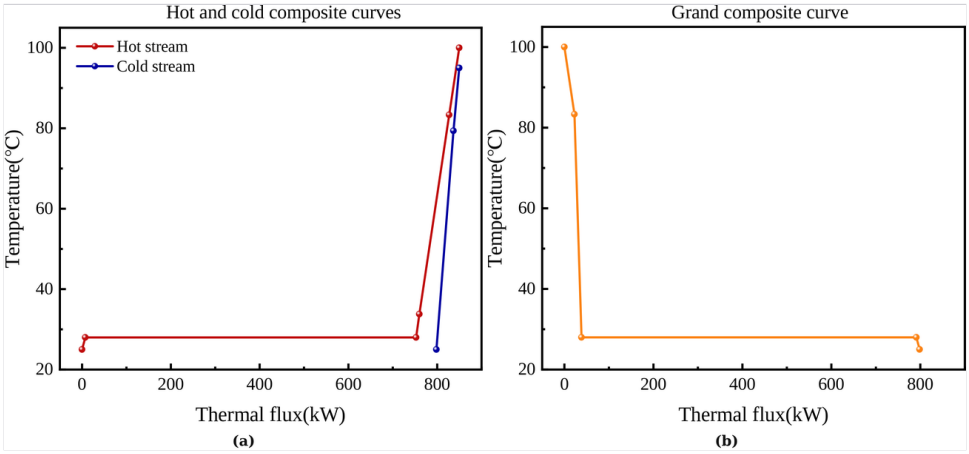

Figure 3. Pinch analysis results for the HEN1 on the dehydrator side: (a) hot and cold composite curves (b) grand composite curve.

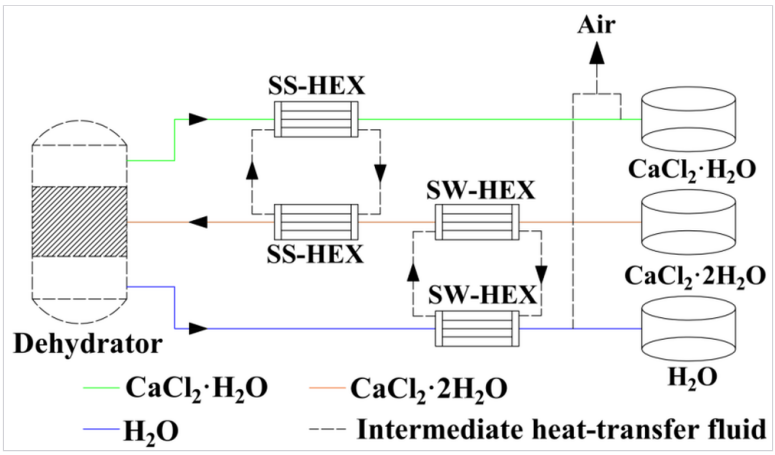

Figure 4. The designed HEN1 in the charging subsystem based on the pinch analysis results.

4.3. Design of heat exchanger networks in the discharging subsystem

As shown in Fig. 5, pinch analysis was conducted for HEN2 to evaluate the heat recovery potential and guide the design of the discharging-side heat exchanger network. The hot streams mainly include the hydration heat and the cooling heat of $CaCl_2{\cdot}2H_2O$, while the cold streams consist of $CaCl_2{\cdot}H_2O$, H_2O, and the ORC working fluid. The overlap between the hot and cold composite curves indicates that internal heat recovery is feasible, particularly in the medium-temperature region, although the temperature difference between the curves still results in heat-transfer irreversibility. Based on the grand composite curve in Fig. 5(b), a considerable heat load can be recovered and redistributed within the discharging subsystem. Therefore, the HEN2 configuration shown in Fig. 6 was designed. In this network, SW-HEXs recover heat between solid and water streams, while SF-HEXs and WF-HEXs transfer heat to the intermediate heat-transfer fluid and ORC working fluid. With the assistance of the auxiliary compressor and water pump, the recovered hydration heat is used for reactant preheating and ORC heat supply, thereby improving heat matching and the energy utilization efficiency of the discharging process.

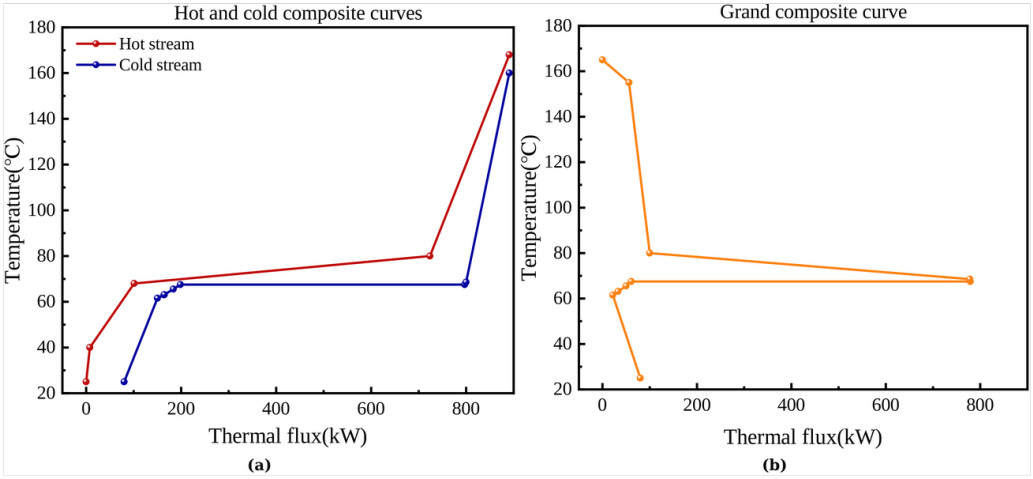

Figure 5. Pinch analysis results for the HEN2 on the hydrator side: (a) hot and cold composite curves (b) grand composite curve.

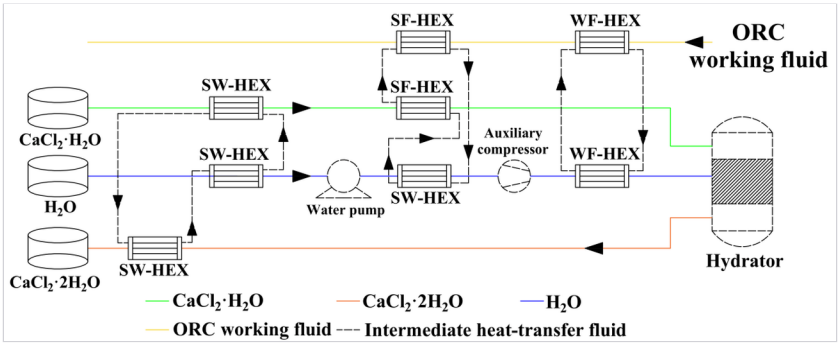

Figure 6. The designed HEN2 in the discharging subsystem based on the pinch analysis.

4.4. Exergy analysis

As shown in Fig. 7(a), the total exergy destruction of the TSC-CB-HEN is 604.24 kW, with significant differences among components. HEX2 exhibits the largest exergy destruction of 211.14 kW, accounting for 34.9% of the total (Fig. 7(b)), mainly due to the strong temperature mismatch in the coupled processes of hydration heat release, water heating/evaporation, reactant preheating, and product cooling. The evaporator shows the second-largest exergy destruction of 93.51 kW, accounting for 15.5%, which is mainly caused by the evaporation process of the working fluid and the temperature difference between the heat source and the working fluid during heat transfer. Reactor 2 and the condenser also contribute considerable exergy destruction, with values of 59.00 kW and 53.73 kW, respectively. According to Eq. (6), the recovered heat of 217.1 kW at a dehydrator temperature of 100 °C corresponds to a recovered thermal exergy of 43.64 kW, resulting in a system exergy efficiency of approximately 63.6%. These results show that improving heat-flow matching in HEX2, reducing terminal temperature differences, and enhancing heat and mass transfer in the reactors are essential for reducing exergy destruction and improving system performance.

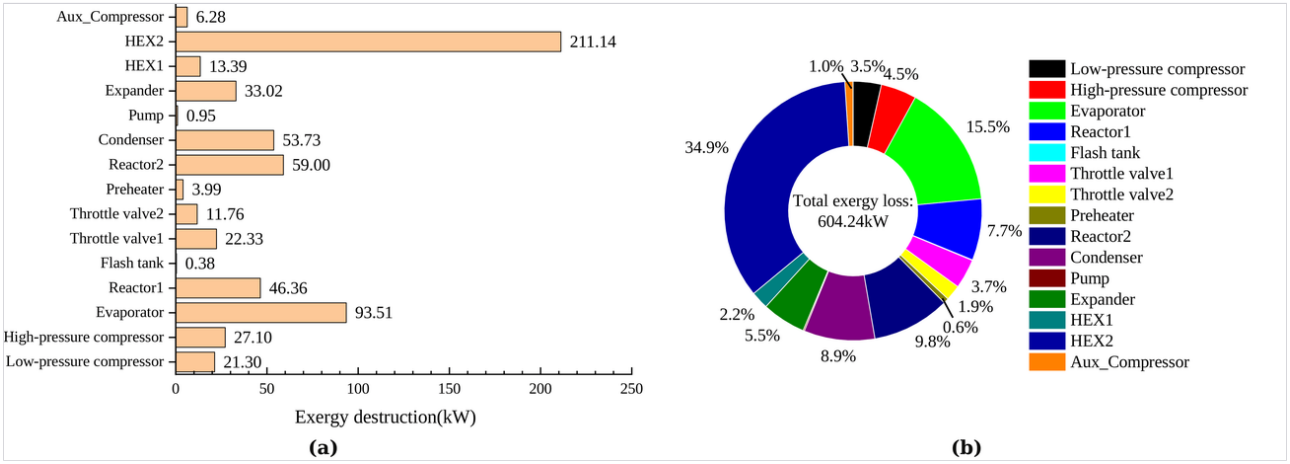

Figure 7. Exergy loss and its proportion across each component of the TSC-CB-HEN: (a) exergy destruction, (b) proportion.

5. Conclusion

This paper proposed and evaluated a salt-hydrate thermochemical Rankine-Carnot battery system integrating $CaCl_2{\cdot}2H_2O/CaCl_2{\cdot}H_2O$ thermochemical energy storage, a heat pump cycle, an organic Rankine cycle, two-stage compression, and heat exchanger networks. By regulating the water vapor pressure, the system enables low-temperature dehydration during charging and higher-temperature hydration during discharging, thus realizing heat quality upgrading. Compared with the SH-CB, the proposed TSC-CB-HEN improves thermodynamic performance by reducing compression power consumption and enhancing internal heat recovery. Under the optimized condition, the COP increases from 3.032 to 3.581, the ORC efficiency increases from 14.5% to 15.0%, and the round-trip efficiency increases from 44.18% to 53.71%.

In the TSC-CB-HEN, the charging HEN1 recovers sensible and latent heat from dehydration products for reactant preheating. On the discharging, the HEN2 mainly recovers sensible heat from product cooling and internal streams, which is used to preheat the reactants before entering the hydration reactor and preheat the ORC working fluid before entering the evaporator. The exergy efficiency reaches approximately 63.6%, with a total exergy destruction of 604.24 kW. HEX2 has the largest exergy destruction of 211.14 kW, accounting for 34.9% of the total, mainly due to temperature mismatch during hydration heat recovery and reactant preheating. Therefore, optimizing the discharging heat exchanger network, reducing terminal temperature differences, and enhancing heat and mass transfer in the reactors should be considered in the future.

Declarations

Author contributions. Xianmin Zeng: Writing (original draft), Data curation, Formal analysis, Investigation, Methodology, Conceptualization. Xianglong Luo: Writing (review and editing). Yingzong Liang: Writing (review and editing). Jianyong Chen: Writing (review and editing). Zhi Yang: Writing (review and editing). Rongjun Wu: Writing (review and editing).

Funding. This research received no specific funding.

Conflicts of interest. The authors declare no competing interests.

Data availability. The data that support the findings of this study are available from the corresponding author upon reasonable request.

References

Albrecht, Kevin J.; Ho, Clifford K. (2019) 'Design and operating considerations for a shell-and-plate, moving packed-bed, particle-to-sCO_2 heat exchanger', *Solar Energy*, 178, pp. 331-340. Available at: https://doi.org/10.1016/j.solener.2018.11.065

Dumont, Olivier; Frate, Guido Francesco; Pillai, Aditya; Lecompte, Steven; De Paepe, Michel; Lemort, Vincent (2020) 'Carnot battery technology: A state-of-the-art review', *Journal of Energy Storage*, 32, pp. 101756. Available at: https://doi.org/10.1016/j.est.2020.101756

Hayatina, Isye; Auckaili, Amar; Farid, Mohammed (2023) 'Review on Salt Hydrate Thermochemical Heat Transformer', *Energies*, 16(12), pp. 4668. Available at: https://doi.org/10.3390/en16124668

Huang, Jiaxing; Zhao, Yao; Song, Jian; Wang, Kai; Zhu, Peiwang; Liu, Bingchi; Sun, Peifeng (2025) 'Thermodynamic investigation of a Joule-Brayton cycle Carnot battery multi-energy system integrated with external thermal (heat and cold) sources', *Applied Energy*, 377, pp. 124652. Available at: https://doi.org/10.1016/j.apenergy.2024.124652

IEA (2025) *Global Energy Review 2025*. Paris: International Energy Agency. Available at: https://www.iea.org/reports/global-energy-review-2025

Kato, Kazuki; Hotta, Mito; Koga, Nobuyoshi (2024) 'Water vapor effect on the physico-geometrical reaction pathway and kinetics of the multistep thermal dehydration of calcium chloride dihydrate', *Physical Chemistry Chemical Physics*, 26(26), pp. 18476-18492. Available at: https://doi.org/10.1039/d4cp01870b

Kur, Anti; Darkwa, Jo; Calautit, John; Boukhanouf, Rabah; Worall, Mark (2023) 'Solid–Gas Thermochemical Energy Storage Materials and Reactors for Low to High-Temperature Applications: A Concise Review', *Energies*, 16(2), pp. 756. Available at: https://doi.org/10.3390/en16020756

Li, Wei; Markides, Christos N.; Zeng, Min; Peng, Jian (2024a) '4E evaluations of salt hydrate-based solar thermochemical heat transformer system used for domestic hot water production', *Energy*, 286, pp. 129602. Available at: https://doi.org/10.1016/j.energy.2023.129602

Li, Wei; Zhang, Lianjie; Deng, Yajun; Zeng, Min (2024b) 'Thermo-economic assessment of a salt hydrate thermochemical energy storage-based Rankine Carnot battery system', *Energy Conversion and Management*, 312, pp. 118564. Available at: https://doi.org/10.1016/j.enconman.2024.118564

Liu, Huawei; Zhang, Yongqing; Xu, Qianghui; Han, Wei; Shen, Jun (2025) 'A Carnot battery system integrating $Ca(OH)_2$/CaO thermochemical energy storage and supercritical CO_2 cycles for long-term energy storage and residential heat supply', *Applied Energy*, 377, pp. 124535. Available at: https://doi.org/10.1016/j.apenergy.2024.124535

Molenda, Margarethe; Stengler, Jana; Linder, Marc; Wörner, Antje (2013) 'Reversible hydration behavior of $CaCl_2$ at high H_2O partial pressures for thermochemical energy storage', *Thermochimica Acta*, 560, pp. 76-81. Available at: https://doi.org/10.1016/j.tca.2013.03.020

Pardo, P.; Anxionnaz-Minvielle, Z.; Rougé, S.; Cognet, P.; Cabassud, M. (2014) '$Ca(OH)_2$/CaO reversible reaction in a fluidized bed reactor for thermochemical heat storage', *Solar Energy*, 107, pp. 605-616. Available at: https://doi.org/10.1016/j.solener.2014.06.010

Pathak, Amar Deep; Nedea, Silvia; Zondag, Herbert; Rindt, Camilo; Smeulders, David (2016) 'A DFT-based comparative equilibrium study of thermal dehydration and hydrolysis of $CaCl_2$ hydrates and $MgCl_2$ hydrates for seasonal heat storage', *Physical Chemistry Chemical Physics*, 18(15), pp. 10059-10069. Available at: https://doi.org/10.1039/c6cp00926c

Richter, Margarethe; Bouché, Martin; Linder, Marc (2016) 'Heat transformation based on $CaCl_2/H_2O$ – Part A: Closed operation principle', *Applied Thermal Engineering*, 102, pp. 615-621. Available at: https://doi.org/10.1016/j.applthermaleng.2016.03.076

Risthaus, Kai; Linder, Marc; Schmidt, Matthias (2022) 'Experimental investigation of a novel mechanically fluidized bed reactor for thermochemical energy storage with calcium hydroxide/calcium oxide', *Applied Energy*, 315, pp. 118976. Available at: https://doi.org/10.1016/j.apenergy.2022.118976

Tariq, Abdul Haseeb; Amin, Uzma (2025) 'Peer-to-peer multi-energy trading in a decentralized network: A review', *Renewable and Sustainable Energy Reviews*, 208, pp. 114969. Available at: https://doi.org/10.1016/j.rser.2024.114969

Vecchi, Andrea; Knobloch, Kai; Liang, Ting; Kildahl, Harriet; Sciacovelli, Adriano; Engelbrecht, Kurt; Li, Yongliang; Ding, Yulong (2022) 'Carnot Battery development: A review on system performance, applications and commercial state-of-the-art', *Journal of Energy Storage*, 55, pp. 105782. Available at: https://doi.org/10.1016/j.est.2022.105782

Wang, Dabiao; Sun, Zihao; Xu, Qianghui; Tian, Ran; Han, Wei; Shen, Jun (2024) 'Thermodynamic modeling and analysis of a Carnot battery system integrating calcium looping thermochemical energy storage with coal-fired power plant', *Energy Conversion and Management*, 318, pp. 118888. Available at: https://doi.org/10.1016/j.enconman.2024.118888

Wang, Zhikang; Li, Yimin; Qiu, Zhijie; Han, Dongjiang; Sui, Jun (2025) 'Thermodynamic and economic analysis of a novel dual-pressure organic Rankine cycle coupled two-stage vapor compression heat pump system', *International Journal of Refrigeration*, 172, pp. 240-255. Available at: https://doi.org/10.1016/j.ijrefrig.2025.01.024

Zhang, Yongqing; Liu, Huawei; Lu, Jia; Xu, Qianghui; Xu, Chao (2025) 'An integrated energy storage system coupling $Ca(OH)_2/CaO/CaCO_3$ thermochemical energy storage, supercritical CO_2 cycle, and CO_2 capture', *Journal of Energy Storage*, 130, pp. 117487. Available at: https://doi.org/10.1016/j.est.2025.117487

Zhao, Guangyao; Li, Zhen; Yao, Jiakang; Zhao, Zhehui; Zhang, Sixing; Cheng, Na; Jiang, Lei; Yan, Jun (2024) 'Improving the Thermochemical Heat Storage Performance of Calcium Hydroxide in a Fixed-Bed Reactor by Y-Shaped Fins', *Buildings*, 14(11), pp. 3694. Available at: https://doi.org/10.3390/buildings14113694

HOW TO CITE THIS PAPER

Zeng, X., Luo, X., Liang, Y., Chen, J., Yang, Z. and Wu, R. (2026). A novel salt hydrate thermochemical Rankine-Carnot battery: system design, heat exchanger network integration, and thermodynamic assessment. In: *Proceedings of the 22nd International Conference on Sustainable Energy Technologies (SET2026)*, Kuala Lumpur, Malaysia, 13 to 15 August 2026. Caravel Press, pp. 95–108. ISBN 978-1-995850-00-9. ISSN 2978-4387. https://doi.org/10.65582/set.2026.008

COPYRIGHT AND LICENCE

© 2026 The Author(s). This is an open access paper distributed under the terms of the Creative Commons Attribution (CC BY 4.0) licence, which permits unrestricted use, distribution and reproduction in any medium, provided the original work is properly cited.

WSSET World Society of Sustainable Energy Technologies Organised by the World Society of Sustainable Energy Technologies. Published by Caravel Press.